Boundary-Layer Meteorol (2011) 141:443–465
DOI 10.1007/s10546-011-9640-2

ARTICLE

Estimating Aerodynamic Parameters of Urban-Like Surfaces with Heterogeneous Building Heights

J. T. Millward-Hopkins · A. S. Tomlin · L. Ma · D. Ingham · M. Pourkashanian

Received: 8 February 2011 / Accepted: 14 July 2011 / Published online: 12 August 2011

Abstract There are many geometrical factors than can influence the aerodynamic parameters of urban surfaces and hence the vertical wind profiles found above. The knowledge of these parameters has applications in numerous fields, such as dispersion modelling, wind loading calculations, and estimating the wind energy resource at urban locations. Using quasi-empirical modelling, we estimate the dependence of the aerodynamic roughness length and zero-plane displacement for idealized urban surfaces, on the two most significant geometrical characteristics; surface area density and building height variability. A validation of the spatially-averaged, logarithmic wind profiles predicted by the model is carried out, via comparisons with available wind-tunnel and numerical data for arrays of square based blocks of uniform and heterogeneous heights. The model predicts two important properties of the aerodynamic parameters of surfaces of heterogeneous heights that have been suggested by experiments. Firstly, the zero-plane displacement of a heterogeneous array can exceed the surface mean building height significantly. Secondly, the characteristic peak in roughness length with respect to surface area density becomes much softer for heterogeneous arrays compared to uniform arrays, since a variation in building height can prevent a skimming flow regime from occurring. Overall the simple model performs well against available experimental data and may offer more accurate estimates of surface aerodynamic parameters for complex urban surfaces compared to models that do not include height variability.

Keywords Aerodynamic roughness length · Displacement height · Heterogeneous array · Surface roughness · Urban surfaces · Vertical wind profiles · Zero-plane displacement

1 Introduction

An understanding of the airflow in the urban boundary layer (UBL) has applications in numerous fields, such as dispersion modelling, wind loading calculations, and estimating the

J. T. Millward-Hopkins · A. S. Tomlin (✉) · L. Ma · D. Ingham · M. Pourkashanian
School of Process, Environmental and Materials Engineering, University of Leeds, Leeds LS2 9JT, UK
e-mail: A.S.Tomlin@leeds.ac.uk

wind energy resource at urban locations. Normally, of most interest to these applications is the surface layer of the UBL that extends from the ground up to a height of about 100–200 m (Britter and Hanna 2003). This can be split further into the inertial sublayer (ISL) and the roughness sublayer (RSL; Raupach et al. 1991). The ISL is the upper of these two layers, and it is characterized by a constant magnitude of shear stress and horizontally homogeneous flow (Grimmond and Oke 1999). Consequently, in neutral stability, the vertical variation of the horizontal mean wind speed (U) in the ISL follows the usual logarithmic law,

$$U(z) = \frac{u_*}{\kappa} \ln\left[\frac{z-d}{z_0}\right] \tag{1}$$

where $\kappa \approx 0.41$ is the von Karman constant (Davidson 2004), u_* is the friction velocity, z is the height above the ground, and the aerodynamic parameters z_0 and d are the aerodynamic roughness length and zero-plane displacement (sometimes referred to as displacement height), respectively. Below the ISL lies the RSL, where the highly heterogeneous flow is predominantly controlled by the local surface geometry (Britter and Hanna 2003). This layer normally extends up to a height of about 2–5h_m (Raupach et al. 1991), where h_m is the mean building height. Studies of airflow in the RSL above rough, vegetated surfaces have shown that the wind profile in this layer differs significantly from the logarithmic profile of the ISL (Garratt 1980; Raupach et al. 1980). Above these types of surfaces, the RSL profile can be modelled by extrapolating the ISL profile downwards with the addition of a particular correction factor (Harman and Finnigan 2007). However, for urban-like surfaces, it has been suggested that U throughout both the RSL and the ISL can be estimated using a single logarithmic profile (down to a height h_m), provided the profile in the RSL has been spatially averaged (Cheng and Castro 2002). Other investigators have also suggested that, in order to describe the spatial average of U (i.e. $\hat{U}$), the logarithmic law can be extended some way into the urban RSL (Rooney 2001; Britter and Hanna 2003). However, care must be taken when choosing the parameters so that they are suitable for describing both the RSL and ISL profiles, and not just the ISL profile alone (Millward-Hopkins et al. 2011).

A number of models (e.g. Raupach 1992, 1994, 1995; MacDonald et al. 1998; Jia et al. 1998; Kastner-Klein and Rotach 2004; Shao and Yang 2005) have been developed that attempt to relate z_0/h_m and d/h_m to the simplified geometrical parameters of the underlying surface; the plan and frontal area densities (λ_p and λ_f, respectively). Specifically, λ_p is defined to be the ratio of building plan area to ground surface area, or $\lambda_\mathrm{p} = A_\mathrm{p}/A_\mathrm{T}$, and λ_f is defined to be the ratio of building frontal area to ground surface area, or $\lambda_\mathrm{f} = A_\mathrm{f}/A_\mathrm{T}$ (see Fig. 1). Few models use more detailed surface geometry descriptors than these as an input, one

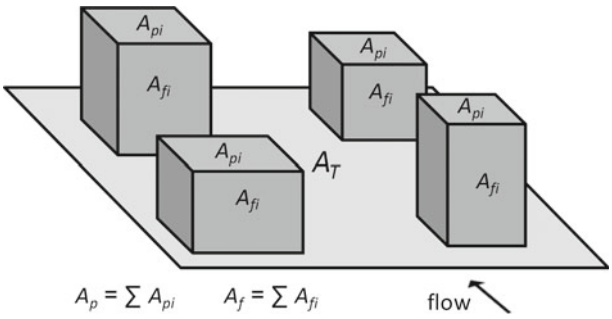

Fig. 1 Illustration of the basic geometric measures: A_p, A_f and A_T

example being that of Bottema (1996, 1997) that uses more complex building layout parameters. However, an issue with using the parameters predicted by the simpler kinds of models in real urban environments is that they are derived for idealized uniform arrays, with blocks equally spaced, aligned normally with the flow, and of uniform height. Another important issue, with respect to model validation, is the difficulty of accurately estimating z_0 and d from measurements, and the inconsistencies between experiments in the methodologies used to estimate these parameters. Consequently, there is large scatter in reported values of z_0 and d, even from wind-tunnel experiments over identical uniform arrays (Grimmond and Oke 1999). As a consequence, a comprehensive review of many of these models (Grimmond and Oke 1999) concluded that, in real urban areas, estimates of both z_0 and d can be highly uncertain.

Examples of geometrical factors that can significantly affect wind profiles above urban surfaces include oblique approaching winds (Hagishima et al. 2009), the addition of pitched roofs to buildings (Rafailidas 1997), and variations in building height (Cheng and Castro 2002; Kanda 2006; Xie et al. 2008; Jiang et al. 2008; Hagishima et al. 2009), all of which have been observed to significantly alter the roughness of a surface. Of all of these geometrical complications, it appears that height variability may be one of the most significant factors influencing surface parameters. However, this factor is not commonly included in models that aim to predict z_0 and d.

As an alternative to using Eq. 1 to estimate $\hat{U}$ profiles in urban areas with height variability, Di Sabatino et al. (2008) developed a model based upon a horizontally-averaged balance equation between the building drag force and the local shear stress. This balance is evaluated from the ground up to a reference height in the ISL and the output is an estimate of the $\hat{U}$ profile throughout the height range. This is potentially more accurate than assuming that the logarithmic profile of the ISL can be extrapolated downwards to estimate the RSL wind profile. However, the model does not explicitly calculate surface aerodynamic parameters. In fact, the input parameters include d and $\mathrm{d}\hat{U}/\mathrm{d}z$, the latter of which can be estimated with a knowledge of z_0. Therefore, to implement this model it is useful to first estimate z_0 and d by another method that is dependent upon λ_p or λ_f (such as those described above).

The aim of our study is to use a simplified modelling approach to explore the simultaneous effects of two highly important geometrical parameters upon z_0 and d, namely building height variability and surface density. The values of z_0 and d output by the model can be used for estimating above-roof $\hat{U}$ profiles. Furthermore, the model can also be used to estimate z_0 and d as an input into more complex models, such as that of Di Sabatino et al. (2008). The structure of the paper is as follows: in Sect. 2, the dependence of aerodynamic parameters upon surface obstacle density and the in-street flow regime is described, followed by a brief description of the modelling approach. In Sect. 3.1, a model for uniform building arrays is derived and validated that is strongly influenced by those of MacDonald et al. (1998), Bottema (1996, 1997) and Raupach (1992, 1994, 1995) (now referred to in short as, Mac98, Bott9697 and R92-95, respectively). In Sect. 3.2, this model is extended to arrays of heterogeneous heights and is validated against available wind-tunnel and numerical data. Finally, in Sect. 4, the main conclusions are summarized.

2 Theory and Modelling Approach

2.1 Flow Regimes and Surface Parameters

It is possible to gain insight into the relationship between surface aerodynamic parameters and the density of buildings covering the surface by considering the three flow regimes described

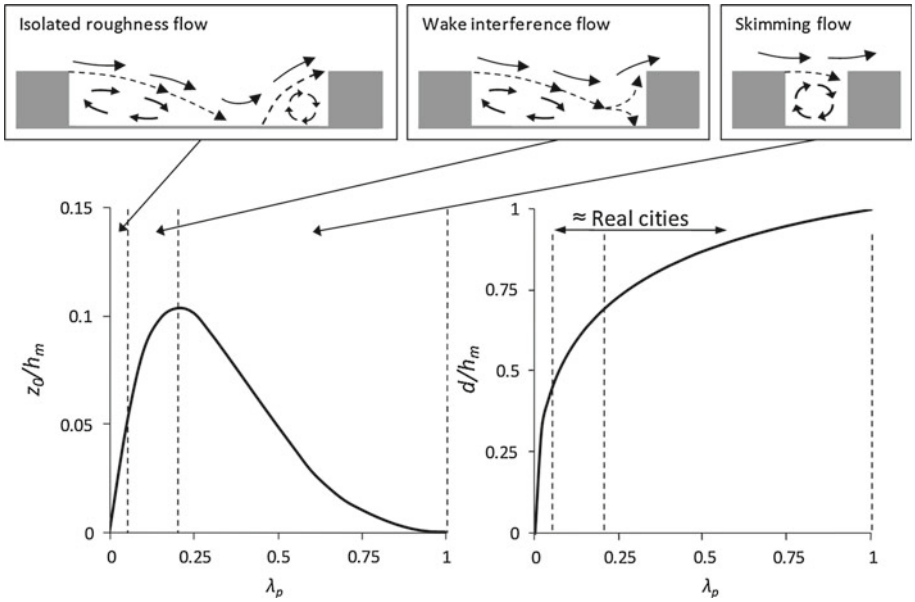

Fig. 2 Curves illustrating, qualitatively, the dependence of the aerodynamic parameters of a surface (z_0 and d) upon λ_p and the three flow regimes described by Oke (1988)

by Oke (1988) after the work of Hussain and Lee (1980). For arrays of uniform height, these relationships are estimated by the curves sketched in Fig. 2. Detailed heuristic arguments for the curves are made by Grimmond and Oke (1999) and therefore only a brief discussion of how these curves relate to the three distinct flow regimes is made.

The first of these regimes, 'isolated roughness flow', occurs at low area densities where the wakes of the individual buildings have negligible interference with the buildings downstream. Associated with this regime are low magnitudes of z_0 and d, which increase with increasing density. Eventually, when the surface becomes sufficiently dense, the building wakes begin to interfere with the downstream buildings, and the flow regime is now referred to as 'wake interference flow'. In this regime there is also an increase in z_0 and d as the density of the surface increases, until at a certain density, z_0 reaches a characteristic peak. As the surface density increases further the flow undergoes transition to the 'skimming flow' regime, in which the main flow effectively skims over the top of the surface elements. The mutual sheltering of the obstacles that occurs under skimming flow increases with the surface density, leading to a reduction in the drag and a decrease in z_0. In this regime, d continues to increase with density, but the rate of increase gradually slows. Eventually, at $\lambda_p = 1$, a new surface is formed of height h_m, hence it follows that d is now equal to h_m.

In real urban arrays, where building height heterogeneity is almost guaranteed, two important characteristics of these curves are no longer valid. Firstly, a variation of building heights may prevent skimming flow from occurring (Di Sabatino et al. 2008). Hence, the characteristic z_0 peak found at the transition from wake interference flow to skimming flow may become softer, and shifted towards higher densities (Hagishima et al. 2009). Secondly, the upper limit for uniform arrays of $d/h_m = 1$ is no longer valid, and for heterogeneous arrays d/h_m has often been found to exceed unity (Cheng and Castro 2002; Jiang et al. 2008; Hagishima et al. 2009). In Sect. 3.2 it will be shown that the model developed in this work is able to capture these characteristics.

2.2 Modelling Approach

Estimates of aerodynamic parameters, z_0 and d, are achieved in this study via a quasi-empirical modelling approach. A model is developed that is centred upon simplified drag balances on the surfaces and physical flow properties that have previously been observed in experiments. Specifically, by considering the balance between the drag force of a surface (F_D) and the shear stress in the ISL ($\tau = \rho u_*^2$; where ρ is the air density), the dependence of roughness length upon area density is estimated. Subsequently, to complete the model, the zero-plane displacement is estimated by considering the vertical profile of the surface drag force. This is first done for uniform arrays, and then similar ideas are extended to arrays of heterogeneous building heights.

3 Results and Discussion

3.1 Modelling Arrays of Uniform Height

3.1.1 The Drag Balance

By considering idealized, uniform arrays of square based blocks (now referred to simply as 'uniform arrays'), it is possible to capture the effects illustrated in Fig. 2. The symmetry of these types of arrays dictates that only one building need be considered, hence F_D is considered to be the drag on a single building. The balance (illustrated in Fig. 3a), simply reads:

$$\rho u_*^2 = F_D / A_T. \tag{2}$$

Bott9697 and Mac98 make two assumptions, firstly that the drag is dominated by the pressure drag of the buildings, and secondly that the logarithmic profile of the ISL can be extended down to the mean building height (h_m). Therefore, any corrections to the RSL profile are assumed to be small enough to neglect. The former assumption was shown by Raupach (1992) to be true for surfaces denser than about $\lambda_p = 0.05$–0.1. Under these assumptions F_D can be written as follows:

$$F_D = 0.5\ \rho \hat{U}_{hm}^2\ C_D\ A_f^* \tag{3}$$

where $\hat{U}_{hm}$ is obtained from Eq. 1 evaluated at h_m, C_D is the depth integrated drag coefficient, and A_f^* is the *unsheltered* frontal area of the building that is illustrated on Fig. 3a–c. The significance of A_f^* is that it is the area assumed to exert pressure drag on the flow. Clearly A_f^* decreases as the surface density increases. Therefore, this parameter is a useful, simplistic way in which to account for the mutual sheltering that occurs with increasing density that avoids having to consider the complex flow patterns that occur within the obstacle arrays. This area is calculated in Sect. 3.1.2.

Substituting Eqs. 1 and 3 into Eq. 2 and rearranging Eq. 2 we obtain:

$$\frac{z_0}{h_m} = \left(1 - \frac{d}{h_m}\right) \exp\left[-\left(0.5 C_D \kappa^{-2} \frac{A_f^*}{A_T}\right)^{-0.5}\right], \tag{4}$$

and to estimate z_0 for a particular surface, and hence the curve of Fig. 2, we must first estimate C_D, d and A_f^*/A_T.

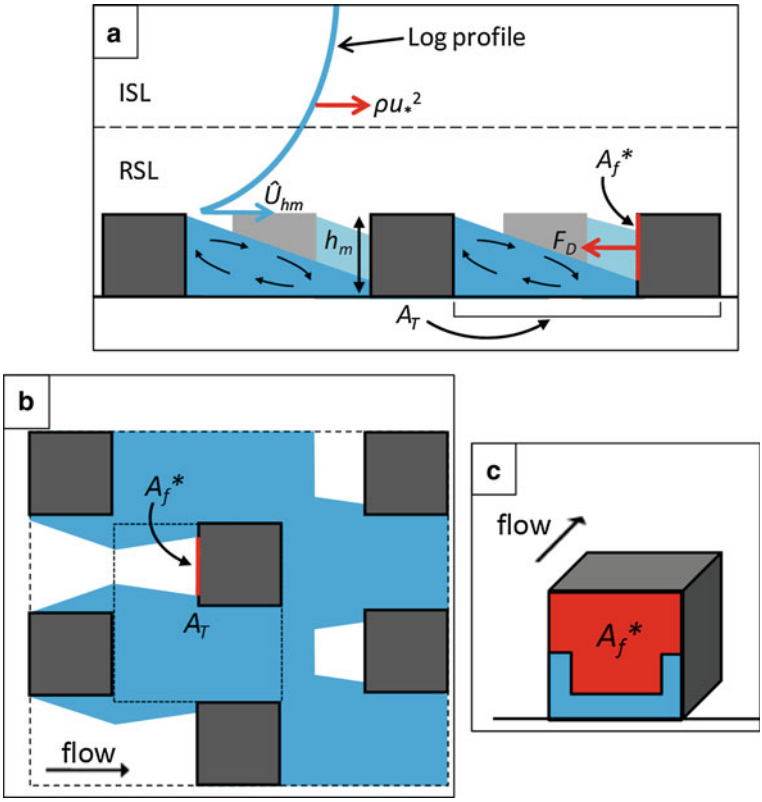

Fig. 3 Illustration of the drag balance calculation for uniform arrays, and the mutual sheltering from the surrounding buildings. Blue areas indicate, approximately, the total sheltered region due to the combined sheltering of all the buildings, and *red* areas indicate the unsheltered frontal area of a single building in the array, A_f^*. **a** Side view; **b** top down view; **c** a single building from the array

Mac98 estimates C_D from the values given by ESDU (1980) for different building shapes and the same approach is followed here. Strictly, these drag coefficients are defined by the height-averaged mean square velocity. However, Mac98 discusses in his work the reasons for using these coefficients as nominal values with a reference velocity at roof level for this type of modelling application. He also makes the assumption that C_D is independent of the surface density (i.e. the shape of A_f^*.) Under these assumptions he obtains satisfactory results, and hence we use these same assumptions here. For cubes a value for C_D of 1.2 is used. To estimate A_f^*/A_T, Mac98 assumes that the drag below a height d is negligible, hence $A_f^*/A_T = \lambda_f(1 - d/h_m)$. However, Bott9697 considers the mutual sheltering due to all the buildings in an array, and this is the approach we take. The method used for estimating d is described in Sect. 3.1.3.

3.1.2 Idealized Descriptions of Individual Building Wakes

In this section a method of approximating the 'effective sheltered volume' of an isolated surface element is described. This volume is intended to enclose the separated regions of flow behind, and on the sides of the building. In reality flow patterns around isolated buildings are highly complex, and become even more so when a building is placed within an array. The

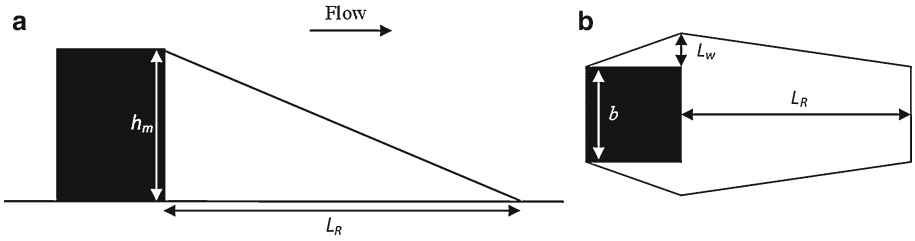

Fig. 4 The shapes and dimensions of the idealized 'effective sheltered volumes' around isolated roughness elements that are used in our study, sketched from **a** the side and **b** above

volume we use here attempts to greatly simplify these effects. Once the shape and size of this volume has been estimated, it is assumed that a large number of surface elements and their effective sheltered volumes are distributed over a surface, as in the work of Bott9697 and R92-95. For uniform arrays it is then simple to estimate the sheltering of a single surface element in the array, and hence obtain an estimate of A_f^* (see Fig. 3).

The surface elements considered are square-based, sharp edged blocks, lying normal to the flow, which are generally used in wind-tunnel simulations of idealized urban areas. Many authors have described in detail the flow pattern that occurs around such an object (Castro and Robins 1977; Hunt et al. 1978; Peterka et al. 1985). In Fig. 4 the idealized sheltered volume used here to describe the sheltering due to this flow pattern is sketched. It can be seen that two parameters govern its shape, namely the rear reattachment length (L_R) and the spanwise extent of sheltering (L_W). Clearly, the most important of these parameters is L_R and, fortunately, established relations exist to describe this length in terms of the building height, width, and depth (h, b and l, respectively). Fackrell (1984) proposed the following empirical expression for L_R, after measuring the parameter for a large variety of different building shapes with b/h ranging from 0.5 to 5 and l/h ranging from 0.3 to 3:

$$\frac{L_R}{h} = \frac{1.8\,(b/h)}{(l/h)^{0.3}\,(1 + 0.24\,(b/h))} \tag{5}$$

where $l = b$ for the square-based blocks considered here. This curve is plotted in Fig. 5a. Although increasing turbulence and shear in the incoming flow are known to decrease the magnitude of L_R (Castro and Robins 1977; Fackrell 1984; Zhang et al. 1993), Eq. 5 was found by Fackrell (1984) to be accurate to within less than $\pm 10\%$ in simulated rural to urban-like boundary layers. Therefore, here it is assumed that L_R/h is dependent only upon the building dimensions.

The assumption of square-based blocks has been made here since available data for arrays of variable height was for this type of geometry. This assumption would not hold if the model was applied to real urban areas, as typically these may have rows of elongated buildings forming street canyons. Eq. 5 could be used to incorporate more complex building shapes since it was found to be valid for a wide variety of building dimensions (Fackrell 1984). However, the complex flow patterns found within urban street canyons such as helical flows (Dobre et al. 2005) cannot be explicitly captured with a simple modelling approach such as that used here. It may be interesting to assess the impact of street canyon type flows in future work, and as new datasets become available. However, our main focus here is to quantify the influence of height heterogeneity on aerodynamic parameters.

The second parameter governing the shape of the idealized shelter volume is L_W, which describes the lateral extent of the sheltering. As with L_R, this parameter can be related to

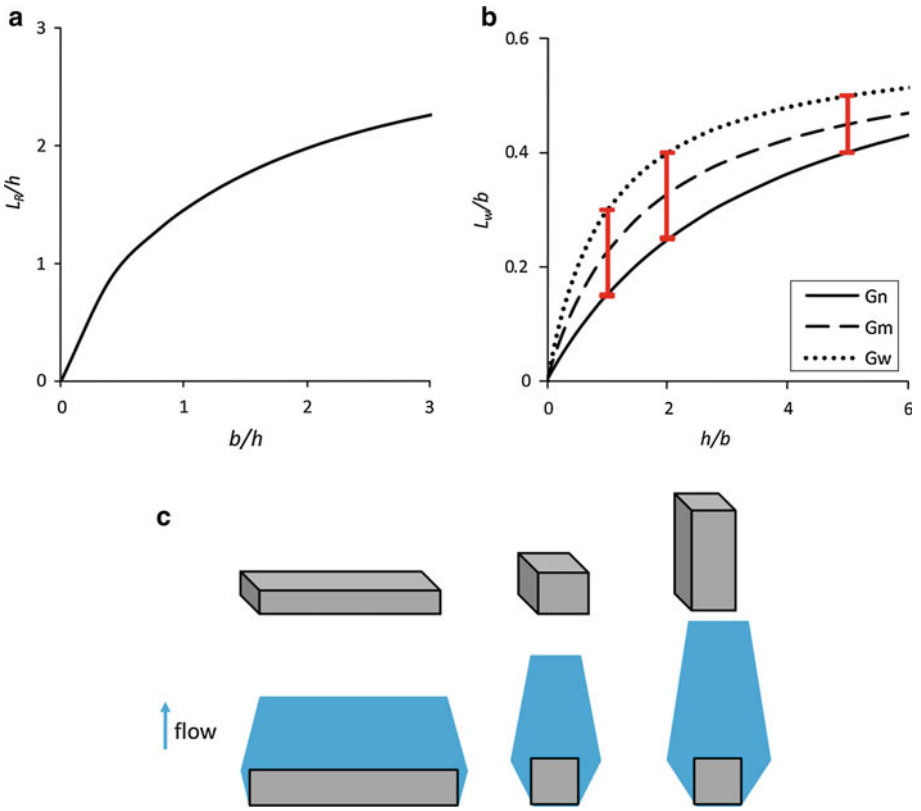

Fig. 5 **a** The relationship between L_R/h and b/h for square-based buildings given by Eq. 5. **b** The relationship between L_W/b and h/b given by Eq. 6. G_n, G_m, and G_w refer to the narrow, medium, and wide curves, respectively, that are used in the model of the current work (each given by Eq. 6, with differing constants). The *red bars* are values estimated from experimental data. **c** Sketch of the sheltered volumes (in *blue*) behind buildings of three different shapes

the building dimensions, however it does not have as clear a criterion as that of L_R, and no standard relation exists to calculate it. Therefore, published data are now used to produce an empirical expression to estimate the dependence of L_W upon the building dimensions.

Intuitively, we would expect L_W to behave as sketched in Fig. 5c. For a very low, wide building, most of the flow that impinges upon the upwind face will be forced over the roof rather than around the sides of the building. Consequently, there will be little lateral displacement of flow relative to the building width, and $L_W/b \approx 0$. As the building becomes taller and narrower, more of the flow becomes displaced around the sides, increasing the magnitude of L_W/b, until it asymptotes to a maximum value and increases no further with increasing building height. Therefore, the relationship between L_W/b and h/b is qualitatively the same as that between L_R/h and b/h, hence a simple empirical relation similar to Eq. 5 is used to describe the dependence of L_W/b upon h/b:

$$\frac{L_W}{b} = \frac{G_1\,(h/b)}{1 + G_2\,(h/b)} \tag{6}$$

where the constants, G_1 and G_2, are chosen to fit published experimental data, which are now described.

Visualization of the flow pattern around a cube in experiments such as that of Rodi (1997) show significant velocity deficits laterally either side of the object to about 15–30% of its width. This suggests that values of $L_W/b \approx 0.15$–0.3 are appropriate for cubes. Similar estimates can be made for taller buildings from other results. These suggest that for buildings with h/b of 2 (Tominag et al. 2008) and 5 (Song and He 1993; Huang et al. 2007), reasonable values for L_W/b are about 0.25–0.4 and 0.4–0.5, respectively. These estimates are shown in Fig. 5b, along with curves fitted centrally, and through the upper and lower limits of these estimates. All three curves use Eq. 6 with differing constants. They are referred to as G_n, G_m, and G_w, which describe narrow, medium, and wide sheltered volumes, respectively. In our study the central curve of G_m is used, where $G_1 = 0.36$ and $G_2 = 0.6$, and the crude choice and construction of this curve is justified by the fact that the model has little sensitivity to the magnitude of L_W/b, provided it is a reasonable value. This is demonstrated in Sect. 3.1.4 using the alternative curves, G_n and G_w.

Using this method of describing the effective shelter volume behind a surface element, an estimate of A_f^* for use in Eq. 4 can be made. Specifically, this estimate is made by first assuming that a particular density of surface elements and their effective sheltered volumes are distributed over a surface as in Fig. 3a and b, then calculating the sheltering of a single surface element in the array to obtain an estimate of A_f^*.

3.1.3 Estimating the Zero-plane Displacement

3.1.3.1 Existing Methods The zero-plane displacement is the final parameter required to estimate z_0 from Eq. 4. To estimate this parameter, each of the models developed by Mac98, Bott9697 and R92-95, use different methods:

(i) Bott9697 estimates d from the ratio V/S, where V is the total volume of buildings and their front and rear recirculation zones, and S is the ground area associated with the buildings. We attempted this method using the current parametrization of sheltered volumes shown in Fig. 4 and the inclusion of front recirculation zones following the method of Bottema. For densities below around $\lambda_p \approx 0.25$ the resulting values of d were found to be significantly lower than those reported from a number of relatively recent wind-tunnel experiments and numerical studies (which are discussed below in due course), and consequently predicted values for z_0 were significantly higher. Increasing the size of the buildings sheltered volumes to the upper limit of what could be considered reasonable did not change the agreement between predicted and experimental vales of z_0 and d significantly.

(ii) Mac98 used an empirical expression for d that was fitted to the experimental data of Hall et al. (1996):

$$\frac{d}{h_m} = 1 + A^{-\lambda_p}\left(\lambda_p - 1\right). \tag{7}$$

For staggered and square arrays, values for the empirical constant, A, of 3.59 and 4.43, respectively, were suggested. However, concerns have been raised regarding the accuracy of the experimental data, primarily due to the relatively short fetch that was used in the wind tunnel and the lack of accurate shear stress measurements (Cheng et al. 2007). Consequently, when compared to more recent experimental data, obtained in fully developed boundary layers using direct shear stress measurements, the equation performs less well.

(iii) Raupach (1992, 1994, 1995) estimates d as the mean height at which the total surface drag force acts, or the drag profile centroid (d_C), motivated by the theoretical arguments of Jackson (1981). The values obtained by Raupach from this method were suggested by Grimmond and Oke (1999) to be reasonable, although relatively low at higher surface densities.

Overall, these different approaches highlight the uncertainty surrounding the physical meaning and calculation of d. However, the theoretical arguments of Jackson (1981) offer an intuitive explanation for d, giving a physical basis to the parameter. Although his theory has not yet been tested over a wide variety of urban-like arrays, we continue under the assumption that the theory is valid. Therefore, we now attempt to determine d by estimating the height of the drag profile centroid.

3.1.3.2 Current Method For uniform surfaces, d_C can be estimated from the following equation:

$$V_{Dc} h_m + \int_0^{h_m} z \mathrm{d}F_D = d_C \left[V_{Dc} + V_{Dg} + \int_0^{h_m} \mathrm{d}F_D \right] \tag{8}$$

where $\mathrm{d}F_D$ is the differential pressure drag force on a surface element at height z, and V_{Dc} and V_{Dg} are viscous drag terms due to the rooftop (i.e. crest) and ground friction, respectively. Physically, the terms on the left-hand side of Eq. 8 represent the total moment of the forces on the surface, and those on the right-hand side represent the total magnitude of forces on the surface multiplied by d_C. A very similar equation is given in Leonardi and Castro (2010), the only difference being that, here, the friction on the building sides is not included. This is because the experiments of Leonardi and Castro (2010) showed its contribution to be relatively insignificant.

The calculation of $\mathrm{d}F_D$ is similar to that of F_D, hence Eq. 3 can be re-written in terms of the 'sectional drag coefficient' (C'_D), which is typically assumed constant with height in flow models (MacDonald 2000; Coceal and Belcher 2004):

$$\mathrm{d}F_D = 0.5\rho\, \hat{U}(z)^2\, C'_D\, (A_f/h_m)\, \mathrm{d}z. \tag{9}$$

To calculate $\mathrm{d}F_D$ an estimate of the $\hat{U}$ profile below the height of the surface elements must be made. This layer is normally referred to as the canopy layer (CL). Here the profile can be well approximated as exponential, although this may break down for surfaces above $\lambda_p \approx 0.3$ (MacDonald 2000):

$$\hat{U}(z) = \hat{U}_{hm} \exp\left[a\,(z/h_m - 1)\right] \tag{10}$$

where a is the attenuation coefficient, which MacDonald (2000) found empirically to be $\approx 9.6\lambda_p$ or $9.6\lambda_f$.

For surfaces denser than $\lambda_p = 0.1$, surface drag is dominated by the pressure drag of the buildings, and the viscous terms, V_{Dc} and V_{Dg}, can be ignored. Therefore, on substituting Eqs. 9 and 10 into Eq. 8 and solving, we obtain:

$$\frac{d_C}{h_m} = \frac{19.2\lambda_p - 1 + \exp\left(-19.2\lambda_p\right)}{19.2\lambda_p\left[1 - \exp\left(-19.2\lambda_p\right)\right]}. \tag{11}$$

For $\lambda_p \geq 0.1$, this equation offers an approximation for d that compares well with various recent experimental datasets. This is demonstrated in Fig. 6a where predictions using Eq. 11

are plotted in red alongside wind-tunnel (Cheng et al. 2007; Hagishima et al. 2009) and numerical data (Jiang et al. 2008; Leonardi and Castro 2010) for uniform arrays. The experimental data are for staggered, square and aligned arrays (st, sq and al, respectively), each of which is illustrated in Fig. 6e. Also the curves from the model of MacDonald et al. (1998) and the more recent model of Kastner-Klein and Rotach (2004) are shown in blue. It can be seen that these model estimates of d are generally much lower than recent experimental data suggests, although the predictions of Kastner-Klein and Rotach (2004) become increasingly more consistent with these experimental data as the area density increases. It is also important to comment on the large scatter that is present in these datasets, particularly at low densities. This highlights the uncertainties in experimentally measured aerodynamic parameters even over relatively simple arrays. In particular, for the experimental data included here, the majority of the scatter appears to derive from the differing height intervals in which aerodynamic parameters were obtained by Hagishima et al. (2009), i.e. they were not always obtained from the ISL where they are theoretically valid. It is also clear from Fig. 6a that an issue with Eq. 11 is that for $\lambda_p < 0.1$ this equation overestimates d and does not tend to the correct limit of $d = 0$ at $\lambda_p = 0$. This is now corrected by estimating the viscous terms in Eq. 8, V_{Dc} and V_{Dg}, for uniform cube arrays.

At low densities, within an isolated roughness flow regime, the drag force on each building is likely to remain approximately constant and V_{Dg} is expected to be proportional to the unsheltered ground area. From Eqs. 5 and 6, the dimensionless, sheltered ground area, due to both the sheltered volume and footprint of a single cube, is $3h^2/A_T$ or $3\lambda_p$. Hence, if V_{Dg} is proportional to the unsheltered ground area it follows that $V_{Dg}/F_D \propto (1-3\lambda_p)/\lambda_p$. Leonardi and Castro (2010) found in their numerical experiments that at $\lambda_p = 0.1$, $V_{Dg} \approx 0.06F_D$, and here this observation is used to calculate the constant of proportionality. Therefore, with F_D given by the integral of $\mathrm{d}F_D$ over the height interval $0 < z < h_m$, we obtain:

$$V_{Dg} = \frac{\rho C'_D A_f \hat{U}^2_{hm} \left[1 - \exp\left(-19.2\lambda_p\right)\right]}{4480\lambda_p} \left(\frac{1 - 3\lambda_p}{\lambda_p}\right). \tag{12}$$

Estimating V_{Dc} is less intuitive since it is strongly dependent upon the rooftop flow pattern as well as the roof shape. However, the results of Leonardi and Castro (2010) show that $V_{Dc}/F_D \propto \lambda_p^2$ is a good approximation for $\lambda_p < 0.2$. When fitting this relationship to their dataset, a constant of proportionality of approximately 1.6 is obtained using the method of least squares. Therefore, with F_D again given by the integral of $\mathrm{d}F_D$ over the building height, we obtain:

$$V_{Dc} = \frac{\rho C'_D A_f \hat{U}^2_{hm} \left[1 - \exp\left(-19.2\lambda_p\right)\right]}{24} \lambda_p. \tag{13}$$

On substituting Eqs. 9 and 10 along with the viscous drag terms of Eqs. 12 and 13 into Eq. 8 and solving we obtain:

$$\frac{d_C}{h_m} = \frac{117\lambda_p + \left(187.2\lambda_p^3 - 6.1\right)\left[1 - \exp\left(-19.2\lambda_p\right)\right]}{\left(1 + 114\lambda_p + 187\lambda_p^3\right)\left[1 - \exp\left(-19.2\lambda_p\right)\right]}. \tag{14}$$

In Fig. 6a it can be seen that at low densities this equation predicts the expected behaviour of d, and predictions also compare well with recent experimental data. At $\lambda_p = 0.1$, both Eqs. 11 and 14 predict very similar zero-plane displacements, but the curves only intercept at $\lambda_p \approx 0.19$.

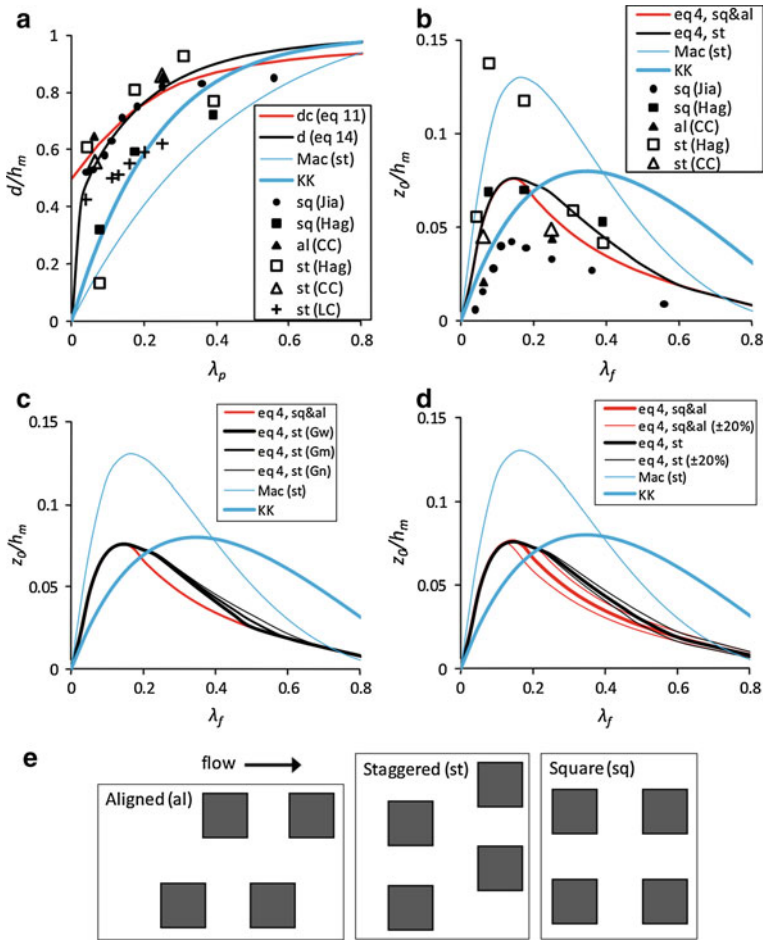

Fig. 6 Estimates of **a** d given by Eqs. 11 and 14, and **b** z_0 given by Eq. 4. The sensitivity of the z_0 predictions of Eq. 4 to **c** the width of the sheltered volume, and **d** the length of the sheltered volume. On **a**–**d** the models of MacDonald et al. (1998) and Kastner-Klein and Rotach (2004) are also shown. **e** Sketches of square, staggered, and inline arrays of cubes. Experimental data from Cheng et al. (2007), Jiang et al. (2008); Hagishima et al. (2009) and Leonardi and Castro (2010), are referred to as CC, Jia, Hag and LC, respectively

Therefore, in the current work, d for uniform arrays is estimated as follows:

$$\frac{d}{h_\mathrm{m}} = \mathrm{f_d}(\lambda_{pi}) = \begin{cases} \dfrac{19.2\lambda_\mathrm{p} - 1 + \exp\left(-19.2\lambda_\mathrm{p}\right)}{19.2\lambda_\mathrm{p}\left[1 - \exp\left(-19.2\lambda_\mathrm{p}\right)\right]} \left(\text{for } \lambda_\mathrm{p} \geq 0.19\right) \\ \dfrac{117\lambda_\mathrm{p} + \left(187.2\lambda_\mathrm{p}^3 - 6.1\right)\left[1 - \exp\left(-19.2\lambda_\mathrm{p}\right)\right]}{\left(1 + 114\lambda_\mathrm{p} + 187\lambda_\mathrm{p}^3\right)\left[1 - \exp\left(-19.2\lambda_\mathrm{p}\right)\right]} \left(\text{for } \lambda_\mathrm{p} < 0.19\right) \end{cases}. \tag{15}$$

This equation is assumed to be independent of the different layouts of surface elements sketched in Fig. 6d, as Cheng et al. (2007) found the centroid of the drag profile to be independent of the building layout.

It is important to comment on any limitations arising from the derivation of Eq. 15. Firstly, it should be highlighted that in Fig. 6a the only experimental data for d derived specifically from the drag centroid are those of Leonardi and Castro (2010). The rest were obtained by traditional best fitting methods. For low densities the agreement between their experimental data and the model predictions is good, but for medium densities their experimental data lie around 20% below the current model predictions. The most likely reason for this is the current model's assumption that C'_{D} is constant with height. It can be seen in the results of Leonardi and Castro (2010) that this assumption becomes less accurate with increasing area density. However, as yet there are no established methods of estimating the profile of C'_{D} and its dependence upon surface geometry. Furthermore, as mentioned previously, the current model predictions of d agree well with the other sources of experimental data.

A second important discussion regarding the model's derivation is the parametrization of the attenuation coefficient. The value of $a \approx 9.6\lambda_{\mathrm{p}}$ suggested by MacDonald (2000) was based upon experiments over square and staggered cube arrays of various densities. However it is possible that a is also influenced by building shape, and hence for arrays of non-cubical buildings that are short and squat, or elongated, more complex parametrisations of a may be required to model d more accurately. Currently however there are few data available regarding the dependence of a upon surface geometry, although if these data were to become available it could be incorporated into the current model with relative ease.

Finally, the method by which viscous forces are incorporated into the model deserves further discussion. Clearly the modelling of these effects is relatively simple, and the empirical observations are from a single experiment. However, overall the surface parameters predicted by the model are only influenced by these simplifications for low densities. Furthermore, for low densities of practical use (about $0.03 < \lambda_{\mathrm{p}} < 0.1$), the predictions are relatively insensitive to the treatment of viscous drag. Taking all of these issues into account we proceed with using Eq. 15 to estimate d, but the limitations and potential improvements to this method should be kept in mind.

3.1.4 Validating the Roughness length Predictions of Uniform Arrays

In Fig. 6b model predictions for z_0 from Eq. 4 are shown, where d has been estimated from Eq. 15. Predictions for staggered, square and aligned arrays are shown, alongside wind-tunnel (Hagishima et al. 2009; Cheng et al. 2007) and numerical data (Jiang et al. 2008). (Note: for square and aligned arrays the predictions are identical). Predictions of z_0 are slightly towards the higher end of the experimental data, however considering the scatter it can be concluded that the model performs well, and the peak roughness occurs at the density suggested by the experiments. Compared to the model of MacDonald et al. (1998), present model predictions for d and z_0 are far more consistent with recent experimental data, most likely due to issues with model calibration as mentioned in the previous section. Agreement between the model of Kastner-Klein and Rotach (2004) and these experimental data is quite poor. However, Kastner-Klein and Rotach (2004) calibrated their model using experimental data obtained from a wind-tunnel study of a scale model of a single European city centre. The height variation that was present may explain the shifted peak in z_0 with respect to the experimental data shown here. Due to this calibration, they specifically warn against applying the model to other urban sites without further considerations.

In Fig. 6c, the model's sensitivity to the width of the sheltered volume is shown using values for L_{W} of $0.15b$, $0.225b$ and $0.3b$, which correspond to the curves G_{n}, G_{m}, and G_{w} shown in Fig. 5b, respectively. It is clear that the model has little sensitivity to this length scale for staggered arrays, and is completely unaffected for square/aligned arrays. Similarly,

to assess the sensitivity of the model to changes in the description of the length of the sheltered volume, in Fig. 6d model predictions are shown with L_R varied by ±20%. A variation of 20% represents about twice the uncertainty found by Fackrell (1984) when using Eq. 5 to estimate L_R and should therefore be a conservative estimate. Clearly the model is more sensitive to L_R than it is to L_W. However, the change in the predictions is still relatively small considering the scatter in the experimental data in Fig. 6b.

3.2 Modelling Arrays of Heterogeneous Height

3.2.1 Modifying the Drag Balance

As the model described in Sect. 3.1 was found to give good predictions of d and z_0 for uniform arrays, similar techniques are now used to adapt it to consider arrays of heterogeneous heights. Again, the model is centred upon the balance between the drag force on a surface and the shear stress in the ISL, however there are two important differences. Firstly, clearly every building in the array must be involved in the calculation. Secondly, it is no longer reasonable to assume that the logarithmic profile of the ISL can be extended into the RSL to estimate the profile of $\hat{U}$ down to a height h_m. Therefore, an 'effective mean building height' ($h_{m\text{-eff}}$), which is greater than h_m, is chosen to be the lower limit of the logarithmic profile extension.

The calculation of $h_{m\text{-eff}}$ is detailed in Sect. 3.2.3, but an important point to make is that it is such that the taller buildings in a heterogeneous array extend above this height (as illustrated in Fig. 7). Consequently, the surface drag force is comprised of a contribution below $h_{m\text{-eff}}$, and a contribution above, referred to as F_{D1} and F_{D2}, respectively. The balance from Eq. 2 now reads:

$$\rho u_*^2 = F_D / A_T = (F_{D1} + F_{D2}) / A_T. \tag{16}$$

Below $h_{m\text{-eff}}$, the drag contribution is estimated by the same method as was used for uniform arrays:

$$F_{D1} = 0.5 \rho \hat{U}_{hm\text{-eff}}^2 \, C_D \, A_f^* \tag{17}$$

for $(h < h_{m\text{-eff}})$, where $\hat{U}_{hm\text{-eff}}$ is the reference wind speed at $h_{m\text{-eff}}$ from Eq. 1, and $A_f^*(h < h_{m\text{-eff}})$ the unsheltered frontal area of the blocks below $h_{m\text{-eff}}$. Strictly, as the buildings below $h_{m\text{-eff}}$ are of different heights, different drag coefficients should be used for each of them.

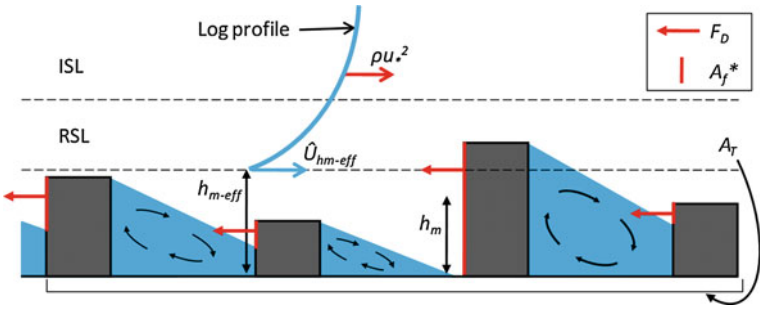

Fig. 7 Sketch of the drag balance for heterogeneous arrays and the mutual sheltering of the buildings. *Blue* areas indicate, approximately, the sheltered regions behind the buildings, and *red* areas indicate the unsheltered frontal area of the buildings, which when summed give A_f^*

However, for simplicity, in Eq. 17 a single value of C_D is chosen that is appropriate for the average building shape. Therefore, for heterogeneous geometries, where the average building shape is a cuboid (i.e. $\lambda_p = \lambda_f$), C_D is chosen to be the same as that used for uniform cube arrays, i.e. $C_D = 1.2$.

Above $h_{\text{m-eff}}$, the drag force can be evaluated by integrating the differential drag force between $h_{\text{m-eff}}$ and the maximum building height ($h_{\max}$):

$$F_{D2} = \int_{h_{\text{m-eff}}}^{h_{\max}} 0.5\rho C'_D \hat{U}(z)^2 \, dA^*_f \tag{18}$$

where $\hat{U}(z)$ is now logarithmic and given by Eq. 1, and again C'_D is the 'sectional drag coefficient'. In the current work, a value for C'_D of 2 is chosen which, for simplicity, remains constant with surface density, as used by Coceal and Belcher (2004). It is well known that C'_D is a difficult parameter to estimate, however the model is not too sensitive to its value. For example, for the arrays referred to below, predicted z_0 values are still in good agreement with the experimental data even when C'_D is increased to 3 (typically z_0 only changes by about 5%).

To obtain an equation that can be used to estimate the roughness length of a heterogeneous array, Eqs. 1, 17 and 18, can be substituted into the drag balance of Eq. 16 and rearranged as follows:

$$2A_T\kappa^2 = C_D\left[\ln\left(\frac{h_{\text{m-eff}} - d}{z_0}\right)\right]^2 A^*_f(h < h_{\text{m-eff}}) + \int_{h_{\text{m-eff}}}^{h_{\max}} C'_D\left[\ln\left(\frac{h-d}{z_0}\right)\right]^2 dA^*_f. \tag{19}$$

As with Eq. 4, Eq. 19 can be used to estimate the roughness length of a heterogeneous array, provided the parameters $A^*_f(h < h_{\text{m-eff}})$, $h_{\text{m-eff}}$ and d, are estimated (although the integral requires that the equation is solved iteratively). The geometric parameter, $A^*_f(h < h_{\text{m-eff}})$, is estimated by considering the mutual sheltering of the individual buildings sheltered volumes (as sketched in Fig. 7), in exactly the same way in which A_f* was previously calculated for uniform arrays. Methods for estimating d and $h_{\text{m-eff}}$ are now described in Sects. 3.2.2 and 3.2.3, respectively.

3.2.2 The Zero-Plane Displacement of Heterogeneous Arrays

An estimate of the zero-plane displacement of heterogeneous arrays cannot easily be made by estimating the drag profile centroid as before. This is due to the fact that the $\hat{U}$ profile from the ground up to the maximum building height is difficult to estimate. Therefore, a different approach is taken, which is now described by considering the simple heterogeneous array sketched in Fig. 8a. Primarily, the zero-plane displacement of a surface is dictated by the flow pattern that occurs within the canopy layer, as different flow patterns raise the height at which the mean drag acts. For the simple heterogeneous array sketched in Fig. 8a, it would be reasonable to suggest that there are effectively two different flow patterns occurring simultaneously. Isolated vortices, characteristic of a SF regime, may be present within the dense lower canopy, while the flow pattern around the sparser tops of the larger blocks may be better described as being in the WIF regime. Accordingly, the canopy may be split into two distinct, uniform horizontal layers (as illustrated). Based upon the density of these layers, Eq. 15 may be used to calculate the zero-plane displacement of each layer, d_1 and d_2, were they to be in isolation. This is done by calculating the height normalized zero-plane

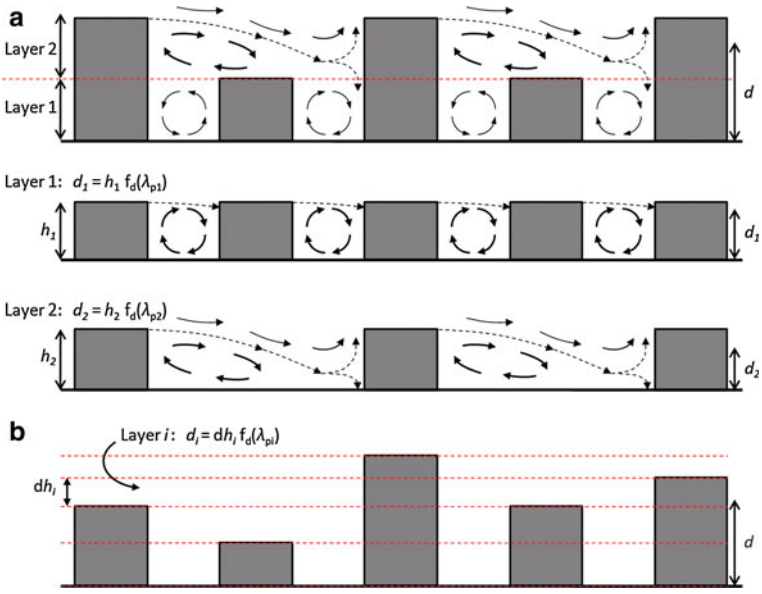

Fig. 8 Illustration of the current method of calculating d for heterogeneous arrays by dividing the canopy into horizontal slices for **a** a simple, repeating heterogeneous array, and **b** any complex heterogeneous array

displacement for each layer and multiplying each value by the thickness of the layer, i.e. $d_1 = h_1 \mathrm{f_d}(\lambda_{p1})$ and $d_2 = h_2 \mathrm{f_d}(\lambda_{p2})$. Furthermore, it may be assumed that when these layers are stacked vertically to obtain the original array, the zero-plane displacement is simply the sum of the values calculated for each layer; $d = d_1 + d_2$.

It is simple to extend this approach to any heterogeneous array by dividing the canopy into sufficiently many distinct, horizontal layers, n, so that each layer is of uniform height, as in Fig. 8b. As these layers have now become quite thin, it is unreasonable to suggest that a different flow pattern occurs within each layer as in Fig. 8a. However, it still seems reasonable to assume that when these layers are stacked vertically to obtain the original heterogeneous array, d can be approximated by taking the height normalized zero-plane displacement of each layer multiplied by the layers thickness; $d_i = \mathrm{d}h_i \mathrm{f_d}(\lambda_{pi})$, and summing over all the layers:

$$d = \sum_{i=1}^{n} \mathrm{d}h_i \; f_d(\lambda_{pi}). \tag{20}$$

Figure 9a and b shows the zero-plane displacements calculated by this method for four heterogeneous surfaces, which are each illustrated in Fig. 9c. ST1.5-st is the two-height surface from the wind-tunnel studies of Hagishima et al. (2009), of area densities: 0.077, 0.174, 0.309 and 0.391; R1.5 is the complex urban-like surface from the wind-tunnel experiments of Zaki et al. (2011), of area densities: 0.077, 0.174, 0.309, 0.391 and 0.481; RM10s is the random height surface of $\lambda_\mathrm{p} = 0.25$ from the wind-tunnel studies of Cheng and Castro (2002). R1, from the numerical studies of Jiang et al. (2008), is a two-height surface of $\lambda_\mathrm{p} = 0.11$, with the normalized standard deviation of the building heights ($\sigma_\mathrm{h}/h_\mathrm{m}$) set to the following values: 0.17, 0.33, 0.5, 0.67 and 0.83, by making the high and low blocks in Fig. 9c gradually higher and lower, respectively. Average height-to-width ratios of the blocks in arrays ST1.5-st, R1.5, RM10s and R1, are 1.5, 1.5, 1 and 1, respectively.

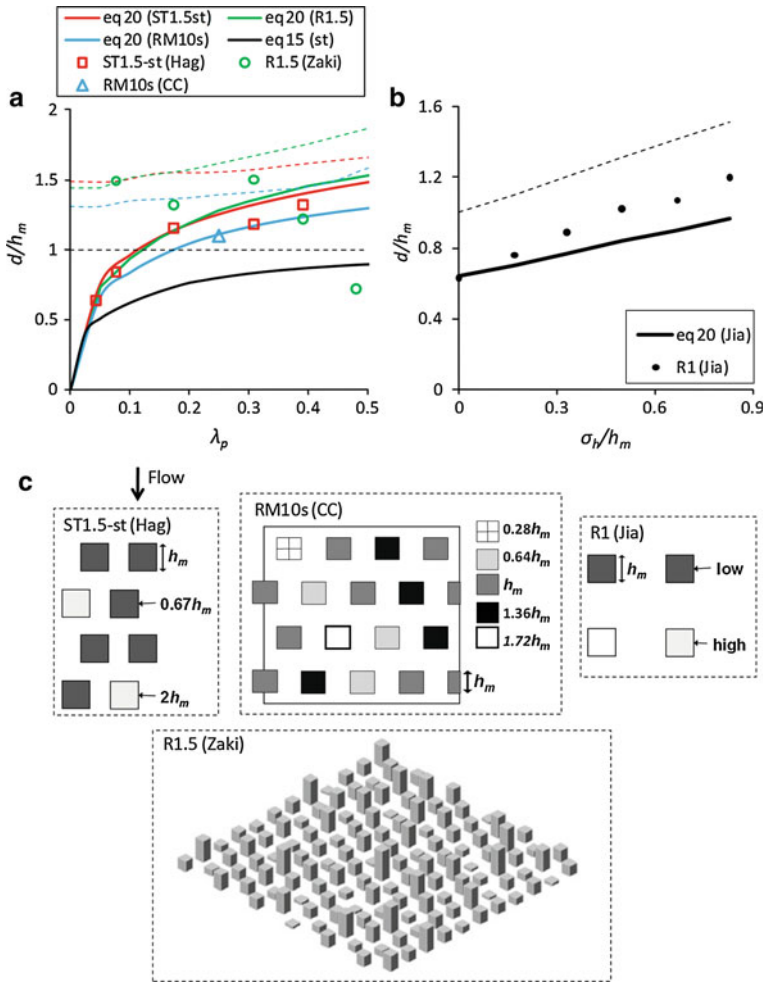

Fig. 9 **a**, **b** Estimates of d given by Eq. 20 and the corresponding experimental results for the arrays illustrated in (**c**). In **a** and **b** the *dashed lines* indicate $h_{\text{m-eff}}$ for each array using appropriate *colour* coding. Experimental data from Cheng and Castro (2002), Jiang et al. (2008), Hagishima et al. (2009) and Zaki et al. (2011), are referred to as CC, Jia, Hag and Zaki, respectively. The illustration in (**c**) for array R1.5 is from Zaki et al. (2011)

It is clear from Fig. 9a and b that zero-plane displacements predicted by Eq. 20 are in very good agreement with the experimental data over the heterogeneous arrays ST1.5-st, RM10s and R1, but over array R1.5 there are significant differences. However, considering the uncertainties that can occur when obtaining z_0 and d from experimental data using statistical best fitting methods, the latter disagreement is not unexpected for such a complex array. Importantly, for all the arrays, Eq. 20 predicts the characteristic that for heterogeneous arrays the magnitude of d can significantly exceed h_{m}.

3.2.3 The Effective Mean Building Height

Within a complex heterogeneous array, it is inaccurate to assume that the $\hat{U}$ profile can be estimated as logarithmic down to h_{m}. Therefore, $h_{\text{m-eff}}$ is chosen to be the lower limit of the

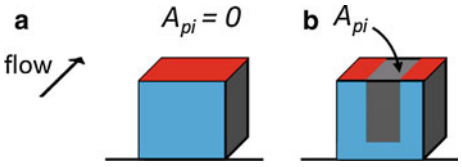

Fig. 10 Examples of individual plan area contributions (A_{pi}) of two sheltered blocks to the 'effective plan area density' ($\lambda_{\text{p-eff}}$) of a heterogeneous array. *Blue* areas indicate the sheltering of the block windward faces by upstream blocks, and *red* areas indicate the plan area *not* contributing to $\lambda_{\text{p-eff}}$

logarithmic profile. To estimate this height, the concept of 'effective plan area density' ($\lambda_{\text{p-eff}}$) is introduced, which is simply the plan area density of a heterogeneous surface *discounting* the sheltered blocks in the array.

The justification for this parameter is that, if a particular heterogeneous array contains low buildings that lie sheltered by larger, upstream buildings, then these have a negligible effect on the above roof flow. Therefore, it may be more appropriate when modelling the above roof profile to ignore any sheltered blocks when calculating the plan area density. Hence we assign the surface a $\lambda_{\text{p-eff}}$ value. Specifically, any block that has its windward face fully sheltered by upstream blocks, as in Fig. 10a, contributes no area to the calculation of $\lambda_{\text{p-eff}}$, and A_{pi} would be zero in Fig. 1. Any block that has its leading edge sheltered, as in Fig. 10b, has its plan area contribution reduced in proportion to this sheltering, since it is the top of the building upwind face that exerts the most drag and influences the above-roof flow most strongly.

To obtain $h_{\text{m-eff}}$ for a particular heterogeneous surface, d and $\lambda_{\text{p-eff}}$ are calculated first via Eq. 20 and the method described in the previous paragraph, respectively. Subsequently, $h_{\text{m-eff}}$ is defined to be the mean building height of the uniform surface of plan area density $\lambda_{\text{p-eff}}$ that would have a zero-plane displacement equal to that of the heterogeneous surface. Hence, since for uniform arrays the logarithmic profile is assumed to be valid down to the mean building height, it is reasonable to consider $h_{\text{m-eff}}$ to be the lowest possible height that a logarithmic profile could be extended down to in a heterogeneous array. To obtain $h_{\text{m-eff}}$, therefore, d and $\lambda_{\text{p-eff}}$ are substituted into a rearranged version of Eq. 15:

$$h_{\text{m-eff}} = \begin{cases} d\dfrac{19.2\lambda_{\text{p-eff}}\left[1-\exp\left(-19.2\lambda_{\text{p-eff}}\right)\right]}{19.2\lambda_{\text{p-eff}}-1+\exp\left(-19.2\lambda_{\text{p-eff}}\right)} & \left(\text{for } \lambda_{\text{p-eff}} \geq 0.19\right) \\ d\dfrac{\left(1+114\lambda_{\text{p-eff}}+187\lambda_{\text{p-eff}}^3\right)\left[1-\exp\left(-19.2\lambda_{\text{p-eff}}\right)\right]}{117\lambda_{\text{p-eff}}+\left(187.2\lambda_{\text{p-eff}}^3-6.1\right)\left[1-\exp\left(-19.2\lambda_{\text{p-eff}}\right)\right]} & \left(\text{for } \lambda_{\text{p-eff}} < 0.19\right) \end{cases} . \tag{21}$$

3.2.4 Validation of the Model for Heterogeneous Arrays

Methods of estimating all of the parameters required to estimate z_0 from Eq. 19 have now been discussed. Hence it is possible to follow these steps and assess the ability of the model to predict z_0 for the arrays sketched in Fig. 9c. A comparison of the model predictions and experimental data for z_0 is shown in Fig. 11a and b. Model predictions of z_0 for staggered cube arrays are also shown (using Eq. 4) to highlight the significantly larger roughness of arrays of random heights compared to arrays of uniform height.

It can be seen that, for arrays ST1.5-st and RM10s, the model predictions are in very good agreement with the experimental data. Compared to uniform arrays, a softer peak in roughness with respect to plan area density is predicted for these heterogeneous arrays. The dip in

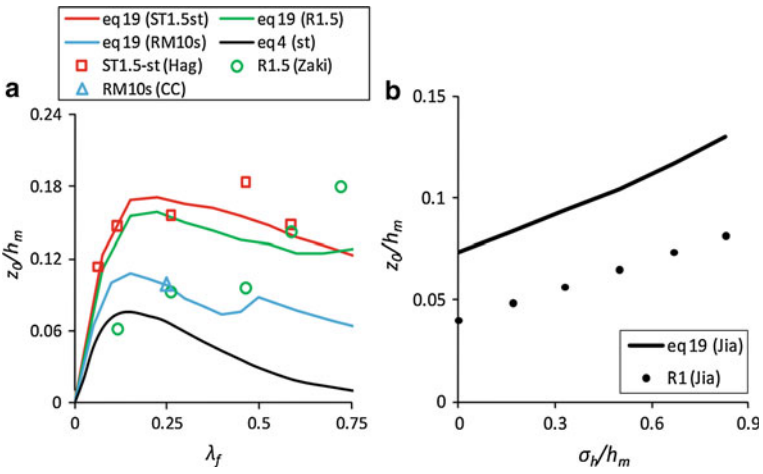

Fig. 11 Estimates of z_0 from Eq. 19 for the arrays illustrated in Fig. 9c and the corresponding experimental results. Experimental data from Cheng and Castro (2002), Jiang et al. (2008), Hagishima et al. (2009) and Zaki et al. (2011), are referred to as CC, Jia, Hag and Zaki, respectively

the z_0 curve for array RM10s at $\lambda_p \approx 0.4$ is simply due to the method of defining $h_{\text{m-eff}}$, as there is a small, but rapid increase in $h_{\text{m-eff}}$ at this density (see Fig. 9a). For the array R1, the experimental data are significantly lower than the model z_0 predictions. However, the numerical data of Jiang et al. (2008) for uniform, square arrays are also significantly lower than the wind-tunnel experiments (see Fig. 6b). Furthermore, the linear rate of increase ofz_0 with increasing building height variation predicted by the model is in very good agreement with the experimental data. For the R1.5 array, the model predictions are significantly different to the experimental data for z_0. This could potentially be due to the uncertainties in obtaining z_0 and d from experimental profiles, as was previously suggested for the d predictions for this array. Specifically, the method used by Zaki et al. (2011) allows for the height interval within which the logarithmic profile is best fit to obtain z_0 and d to vary with area density. This means that, for higher area densities, z_0 and d may have been obtained from the RSL and ISL profiles, while for lower densities they may have been obtained, correctly, from the ISL profile only. This may possibly explain the reduction in d with increasing λ_p found by them, which contradicts the generally accepted view that d increases monotonically with λ_p. Furthermore, these low d estimates at higher area densities would result in estimates of z_0 being biased towards higher values.

It is useful to also compare the $\hat{U}$ profiles measured in these experiments with the logarithmic profiles predicted by the model, although it should be emphasized here that various pairs of z_0 and d can give quite similar wind profiles. A number of comparisons are shown in Fig. 12, for arrays ST1.5-st, RM10s, R1 and R1.5. Profiles plotted using the parameters of the model of MacDonald et al. (1998) are also shown for comparison as, although there were potentially some issues with the models calibration, this model gives reasonably accurate estimates of wind profiles above uniform cube arrays.

From Fig. 12a and b it is apparent that, down to a height of $h_{\text{m-eff}}$ as intended, the predicted logarithmic $\hat{U}$ profiles and the measured $\hat{U}$ profiles are in excellent agreement for array ST1.5-st and RM10s. Furthermore, the inflection points in the profiles from the experimental data are at almost the same height as the values of $h_{\text{m-eff}}$ predicted by the model, suggesting that it is reasonable to consider $h_{\text{m-eff}}$ as the lower limit of the validity of the logarithmic

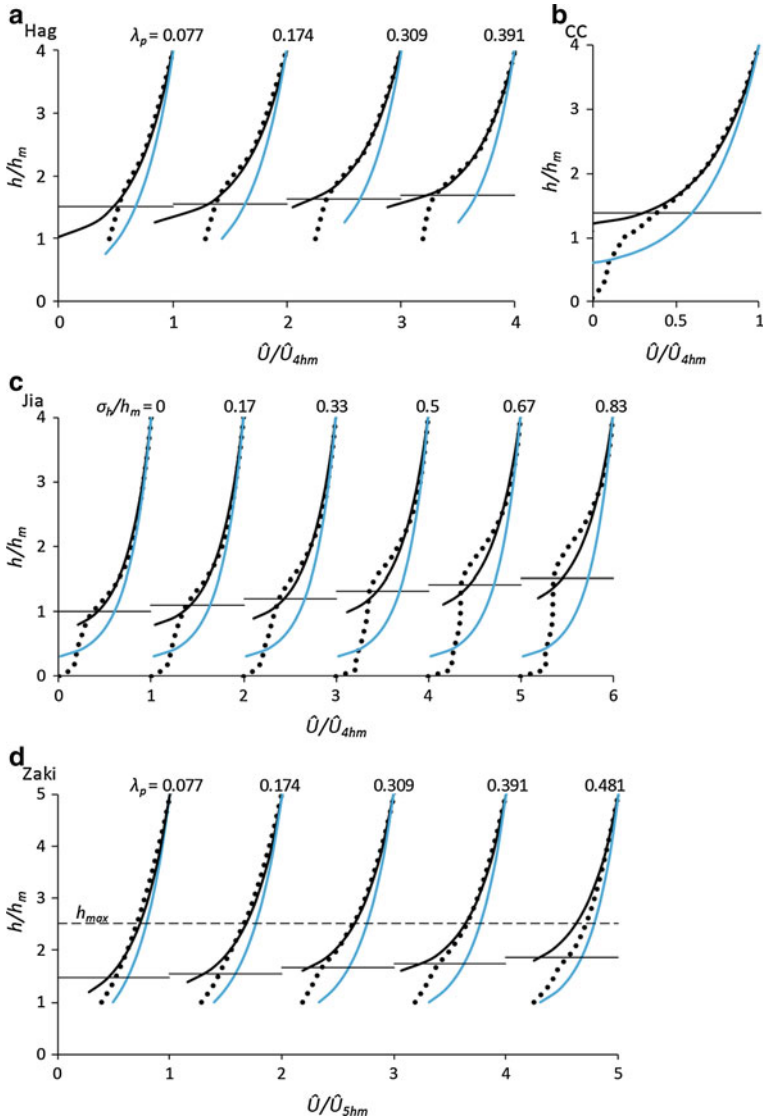

Fig. 12 Logarithmic $\hat{U}$ profiles predicted by the model (*sold lines*) over arrays **a** ST1.5-st, **b** RM10s, **c** R1 and **d** R1.5. Shown for comparison are the $\hat{U}$ profiles (*dotted lines*) from the experiments, and the predictions of the model of MacDonald et al. (1998) (*blue lines*). The *solid horizontal lines* indicate $h_{\text{m-eff}}$. In **a**–**c** profiles are normalized by $\hat{U}$ at $4h_{\text{m}}$, and in (d) by $\hat{U}$ at $5h_{\text{m}}$. Profiles are offset 1 unit for clarity of presentation

profile. In Fig. 12c it can be seen that for array R1, the predicted and measured $\hat{U}$ profiles diverge slightly as σ_{h} increases. However, the agreement is still good for $\sigma_{\text{h}}/h_{\text{m}} = 0.5$, which is the greatest magnitude of height variability found in many major cities (Ratti et al. 2002). Furthermore, again the inflection points in the profiles from the experimental data are at a similar height as the values of $h_{\text{m-eff}}$ predicted by the model. Over array R1.5, the predicted and measured $\hat{U}$ profiles are in excellent agreement, down to a height just above

$h_{\text{m-eff}}$. This is despite the fact that the predictions of z_0 and d differ significantly from the experimental values. The exception is for the highest density surface, $\lambda_p \approx 0.48$, where the model predictions of the measured $\hat{U}$ profile become less accurate. This perhaps highlights a level of density and height heterogeneity at which it is no longer reasonable to describe the $\hat{U}$ profile in the RSL by a downwards extension of the ISL logarithmic law. It is likely as well that at this point some model assumptions break down, such as the description of the idealized shelter volumes and the chosen drag coefficients. It is also clear from Fig. 12 that MacDonald's model significantly overestimates wind profiles above these heterogeneous arrays. This highlights the large inaccuracies that could occur when a model that does not consider height variation is incorrectly used to estimate wind profiles above these types of surfaces.

4 Conclusions

A model has been developed to produce a first estimate of the simultaneous effects of building height variability and surface area density upon the aerodynamic parameters of surfaces (z_0 and d), in order to estimate the profile of spatially-averaged, horizontal mean wind speed ($\hat{U}$) throughout the RSL and ISL, using a logarithmic profile. The model is influenced strongly by those of MacDonald et al. (1998); Raupach (1992, 1994, 1995) and Bottema (1996, 1997). It has built upon their work to include the influences of building height variability, which is one of the most significant geometric factors influencing surface parameters.

Firstly, a model was developed for uniform arrays that predicted the aerodynamic parameters suggested by recent experiments reasonably well, with the peak roughness occurring at the correct density. Subsequently, the model was extended to arrays of heterogeneous building heights and, over a number of heterogeneous arrays, the predicted aerodynamic parameters compared well with wind-tunnel and numerical data. Specifically, two important characteristics were captured. Firstly, the peak in z_0 with respect to surface density for heterogeneous arrays becomes softer when compared to uniform arrays. Secondly, d can exceed the mean building height significantly for heterogeneous arrays. Furthermore, the logarithmic profiles predicted by the model were generally in good agreement with the profiles of $\hat{U}$ from the experimental data down to the 'effective mean building height' ($h_{\text{m-eff}}$), which is a model output.

Overall, the current model offers good estimates of z_0 and d, and hence $\hat{U}$ profiles above heterogeneous surfaces, particularly when compared to models that do not consider height variability. However, the validation has also shown that the predicted $\hat{U}$ profiles become less accurate for surfaces that are either too highly heterogeneous, or too dense. There may also be other limitations of the model that require consideration before it is used in real urban areas due to some of the assumptions made in its derivation, as the current validation has been restricted to arrays of square-based blocks. It would be informative to extend the model validation in the future to arrays with both variable height and building shape. However, for practical use, in future work the model will be applied to various realistic urban arrays in order to suggest simple morphological methods, relying on basic measures of height variation, to estimate the effect of height variability on surface aerodynamic parameters.

Acknowledgments The authors would like to thank Professor Castro, Dr Xie, Professor Hagishima, and Sheikh Ahmad Zaki, for providing the datasets that have been valuable in the validation of our work. They

would also like to thank Engineering and Physical Sciences Research Council for providing the Doctoral Training Award that supported J. T. Millward-Hopkins during the research.

References

Bottema M (1996) Roughness parameters over regular rough surfaces: experimental requirements and model validation. J Wind Eng Ind Aerodyn 64:249–265

Bottema M (1997) Urban roughness modelling in relation to pollutant dispersion. Atmos Environ 31:3059–3075

Britter RE, Hanna SR (2003) Flow and dispersion in urban areas. Annu Rev Fluid Mech 35:469–496

Castro IP, Robins AG (1977) Flow around a surface-mounted cube in uniform and turbulent streams. J Fluid Mech 79:307–335

Cheng H, Castro IP (2002) Near wall flow over urban-like roughness. Boundary-Layer Meteorol 104:229–259

Cheng H, Hayden P, Robins AG, Castro IP (2007) Flow over cube arrays of different packing densities. J Wind Eng Ind Aerodyn 95:715–740

Coceal O, Belcher SE (2004) A canopy model of mean winds through urban areas. Q J Roy Meteorol Soc 130:1349–1372

Davidson PA (2004) Turbulence: an introduction for scientists and engineers. Oxford University Press, Oxford, UK, 655 pp

Di Sabatino S, Solazzo E, Paradisi P, Britter R (2008) A simple model for spatially-averaged wind profiles within and above an urban canopy. Boundary-Layer Meteorol 127:131–151

Dobre A., Arnold SJ, Smalley RJ, Boddy JWD, Barlow JF, Tomlin AS, Belcher SE (2005) Flow field measurements in the proximity of an urban intersection in London, UK. Atmos Environ 39:4647–4657

ESDU (1980) Mean fluid forces and moments on rectangular prisms: surface-mounted structures in turbulent shear flow. Engineering Sciences Data Unit Item Number 80003

Fackrell JE (1984) Parameters characterising dispersion in the near wake of buildings. J Wind Eng Ind Aerodyn 16:97–118

Garratt JR (1980) Surface influence upon vertical profiles in the atmospheric near-surface layer. Q J Roy Meteorol Soc 106:803–819

Grimmond CSB, Oke TR (1999) Aerodynamic properties of urban areas derived, from analysis of surface form. J Appl Meteorol 38:1262–1292

Hagishima A, Tanimoto J, Nagayama K, Meno S (2009) Aerodynamic parameters of regular arrays of rectangular blocks with various geometries. Boundary-Layer Meteorol 132:315–337

Hall D, Macdonald JR, Walker S, Spanton AM (1996) Measurements of dispersion within simulated urban arrays—a small scale wind tunnel study, BRE Client Report, CR178/96

Harman I, Finnigan J (2007) A simple unified theory for flow in the canopy and roughness sublayer. Boundary-Layer Meteorol 123:339–363

Huang S, Li QS, Xu S (2007) Numerical evaluation of wind effects on a tall steel building by CFD. J Constr Steel Res 63:612–627

Hunt JCR, Abell CJ, Peterka JA, Woo H (1978) Kinematical studies of the flows around free or surface-mounted obstacles; applying topology to flow visualization. J Fluid Mech 86:179–200

Hussain M, Lee BE (1980) A wind-tunnel study of the mean pressure forces acting on large groups of low-rise buildings. J Wind Eng Ind Aerodyn 6:207–225

Jackson PS (1981) On the Displacement Height in the Logarithmic Velocity Profile. J Fluid Mech 111(Oct):15–25

Jia YQ, Sill BL, Reinhold TA (1998) Effects of surface roughness element spacing on boundary-layer velocity profile parameters. J Wind Eng Ind Aerodyn 73:215–230

Jiang DH, Jiang WM, Liu HN, Sun JN (2008) Systematic influence of different building spacing, height and layout on mean wind and turbulent characteristics within and over urban building arrays. Wind Struct 11:275–289

Kanda M (2006) Large-eddy simulations on the effects of surface geometry of building arrays on turbulent organized structures. Boundary-Layer Meteorol 118:151–168

Kastner-Klein P, Rotach MW (2004) Mean flow and turbulence characteristics in an urban roughness sublayer. Boundary-Layer Meteorol 111:55–84

Leonardi S, Castro IP (2010) Channel flow over large cube roughness: a direct numerical simulation study. J Fluid Mech 651:519–539

MacDonald RW (2000) Modelling the mean velocity profile in the urban canopy layer. Boundary-Layer Meteorol 97:25–45

MacDonald RW, Griffiths RF, Hall DJ (1998) An improved method for the estimation of surface roughness of obstacle arrays. Atmos Environ 32:1857–1864
Millward-Hopkins JT, Tomlin AS, Ma L, Ingham D, Pourkashanian M (2011) The predictability of the above roof wind resource in the urban roughness sublayer. Wind Energy. doi:10.1002/we.463
Oke TR (1988) Street Design and Urban Canopy Layer Climate. Energy Build 11:103–113
Peterka JA, Meroney RN, Kothari KM (1985) Wind flow patterns about buildings. J Wind Eng Ind Aerodyn 21:21–38
Rafailidas S (1997) Influence of building areal density and roof shape on the wind characteristics above a town. Boundary-Layer Meteorol 85:255–271
Ratti C, Di Sabatino S, Britter R, Brown M, Caton F, Burian S (2002) Analysis of 3-D urban databases with respect to pollution dispersion for a number of European and American cities. Water Soil Air Pollut Focus 2:459–469
Raupach MR (1992) Drag and drag partition on rough surfaces. Boundary-Layer Meteorol 60:375–395
Raupach MR (1994) Simplified expressions for vegetation roughness length and zero-plane displacement as functions of canopy height and area index. Boundary-Layer Meteorol 71:211–216
Raupach MR (1995) Corrigenda. Boundary-Layer Meteorology 76:303–304
Raupach MR, Thom AS, Edwards I (1980) A wind tunnel study of turbulent-flow close to regularly arrayed rough surfaces. Boundary-Layer Meteorol 18:373–397
Raupach MR, Antonia RA, Rajagopalan S (1991) Rough-wall turbulent boundary layers. Appl Mech Rev 44:1–25
Rodi W (1997) Comparison of LES and RANS calculations of the flow around bluff bodies. J Wind Eng Ind Aerodyn 71:55–75
Rooney GG (2001) Comparison of upwind land use and roughness length measured in the urban boundary layer. Boundary-Layer Meteorol 100:469–486
Shao Y, Yang Y (2005) A scheme for drag partition over rough surfaces. Atmos Environ 39:7351–7361
Song CCS, He J (1993) Computation of wind flow around a tall building and the large-scale vortex structure. J Wind Eng Ind Aerodyn 46(47):219–228
Tominag Y, Mochida A, Murakami S, Sawaki S (2008) Comparison of various revised k–e models and LES applied to flow around a high-rise building model with 1:1:2 shape placed within the surface boundary layer. J Wind Eng Ind Aerodyn 96:389–411
Xie ZT, Coceal O, Castro IP (2008) Large-eddy simulation of flows over random urban-like obstacles. Boundary-Layer Meteorol 129:1–23
Zaki S, Hagishima A, Tanimoto J, Ikegaya N (2011) Aerodynamic parameters of urban building arrays with random geometries. Boundary-Layer Meteorol 138:99–120
Zhang YQ, Huber AH, Arya SPS, Snyder WH (1993) Numerical simulation to determine the effects of incident wind shear and turbulence level on the flow around a building. J Wind Eng Ind Aerodyn 46(47):129–134